

Supercritical CO₂ fracturing with different drilling depths in shale

Hongwei Yang, Yuan Zhao, Xinghua Zhang, Guojun Liu, Xidong Du, Deilei Shang, Yongjun Yu, Juan Chen, Hui Wang & Huaijian Tu

To cite this article: Hongwei Yang, Yuan Zhao, Xinghua Zhang, Guojun Liu, Xidong Du, Deilei Shang, Yongjun Yu, Juan Chen, Hui Wang & Huaijian Tu (2019): Supercritical CO₂ fracturing with different drilling depths in shale, Energy Sources, Part A: Recovery, Utilization, and Environmental Effects, DOI: [10.1080/15567036.2019.1673850](https://doi.org/10.1080/15567036.2019.1673850)

To link to this article: <https://doi.org/10.1080/15567036.2019.1673850>



Published online: 10 Oct 2019.



Submit your article to this journal [↗](#)



Article views: 9




View related articles [↗](#)



View Crossmark data [↗](#)



Supercritical CO₂ fracturing with different drilling depths in shale

Hongwei Yang^a, Yuan Zhao ^{b,c,d}, Xinghua Zhang^e, Guojun Liu^f, Xidong Du^g, Deilei Shang^h, Yongjun Yu^b, Juan Chenⁱ, Hui Wang^c, and Huaijian Tu^b

^aState Key Laboratory of Coal Mine Safety Technology, CCTEG Shen yang Research Institute, Fushun, China;

^bSinohydro Bureau 8 Co. LTD., POWERCHINA, Changsha, China; ^cState Key Laboratory of Coal Mine Disaster Dynamics and Control, College of Resource & Environmental Science, Chongqing University, Chongqing, China;

^dInstitute of Mechanics, Chinese Academy of Sciences, Beijing, China; ^eSchool of Safety Technology and Equipment, Taiyuan University of Technology, Taiyuan, China; ^fCollege of Environment and Resources, Xiangtan University, Xiangtan, China;

^gSchool of Earth Sciences, East China University of Technology, Nanchang, China; ^hDepartment of Civil Engineering, Tsinghua University, Beijing, China; ⁱNational Local Joint Engineering Laboratory of Marine Mineral Resources Exploration Equipment and Safety Technology, Hunan University of Science and Technology, Xiangtan, China

ABSTRACT

Shale gas is a crucial unconventional natural gas; carbon dioxide is a serious greenhouse gas. Therefore, using supercritical carbon dioxide as a fracturing fluid can fracture shale reservoirs and exploit shale gas as well as store carbon dioxide to slow the greenhouse effect. In this study, supercritical carbon dioxide fracturing experiments were conducted at different drilling depths. They showed that structural failure pressure decreased with the increase in borehole and sealing lengths owing to the larger excavation damage zone induced by borehole drilling. During the fracturing process, acoustic emission signals were recorded, which exhibited similar development tendencies, and this process could be divided into four parts based on the acoustic emission characteristic. The saltation of fluid pressure was due to the saltation of isothermal compression and expansion occurring in phase change processes. Moreover, crack morphology before and after the fracturing were scanned and rebuilt by computed tomography instruments, which displayed that an effective fracturing crack could be generated by supercritical carbon dioxide. Although the crack morphology was relatively simple, a complex crack could be formed at a deep drilling depth as revealed by the comparisons of the box dimension, crack perimeter, and crack area at different drilling depths. Based on the acoustic emission accumulation counts, a damage variable was introduced to describe failure degree. Furthermore, based on a previous work and the damage characteristic and fluid pressure features, the entire process of supercritical carbon dioxide fracturing could be divided into five main stages. In addition, the chemical reaction between the shale matrix and the fracturing fluid was analyzed. The supercritical fracturing fluid could dissolve and remove substances, improving the shale porosity and connectivity.

ARTICLE HISTORY

Received 21 March 2019

Revised 5 July 2019

Accepted 13 July 2019

KEYWORDS

Acoustic emission; fracturing; supercritical CO₂; damage characteristic; crack morphology

Introduction

Shale is an important reservoir of unconventional gases (Xu et al. 2016; Yuan, Luo, and Feng 2015), and shale gas has been attracting more focus as a significant source of natural gas since it was started to extract in the United States (Stephenson 2016; Wang and Li 2016; Yap 2016). With the development and improvement of the theory and technology of drilling and fracturing (Zhao et al. 2018b, 2019), shale gas has exhibited large-scale commercial exploitation and production value (Cao, Liu, and Leong 2016; Zhang et al.

2015; Zhu, Yuan, and Luo 2016). China also shows one of the most potentials for exploiting and developing shale gas with its reserves of approximately $2.07 \times 10^{14} \text{ m}^3$ (Li et al. 2016; Zhao et al. 2015; Zou et al. 2015). However, most of the reservoirs in China have distinctive features of a high clay content, low or ultra-low permeability, and low-porosity (Sun et al. 2017); therefore, it is necessary to develop the theory, apparatus, and technology of shale gas exploitation. As a solution for the disadvantages of water blockage, waste, and contamination of hydraulic fracture, recently, some scholars proposed supercritical CO_2 as a new type of fracturing fluid (Cheng et al. 2013; Cheng et al. 2014; Du et al. 2011; Kubala and Mackay 2010; Liteanu and Spiers 2011; Middleton et al. 2014; Wang, Li, and Shen 2012; Zhao et al. 2015), and the phase state features show that the supercritical CO_2 phase transition conditions can be readily reached, as exhibited in Figure 1. Fang et al. (2014) simulated fracturing involving pressurized cracks using supercritical CO_2 , water, and slick water as fracturing fluids with the Universal Distinct Element Code software, and found that using supercritical CO_2 as the fracturing fluid had a more effective, economic, and environmental significance. Zhou et al. (2016) conducted a series of experiments of fracturing, computed tomography (CT) scanning, and permeability tests, which indicated that supercritical CO_2 could generate complex fractures and increased the shale permeability considerably. Zhang et al. (2016) performed some experimental research on fracturing and crack propagation with different fracture fluids: water, L (low)- CO_2 , and supercritical CO_2 , under different stress differences, and found that using supercritical CO_2 could increase the fracture conductivity and shale gas production. Ishida et al. (2012) conducted hydraulic fracturing experiments with supercritical CO_2 in granite blocks monitored by an acoustic emission (AE) instrument, and exhibited that supercritical CO_2 fluid generated cracks extending more in a three-dimensional plane rather than a flat plane. Moreover, the breakdown pressures were considerably lower with it than with other fracturing fluids. Zhang et al. (2013) focused on the fracturing principle, generational and carrying capacities, and anti-reflection effect, and analyzed the characteristics of a coal reservoir and coalbed gas and the feasibility and necessity of using supercritical CO_2 as the fracturing fluid in coalbeds. Guo and Zeng (2015) proposed a coupling model of the wellbore transient temperature and pressure of fracturing using supercritical CO_2 based on the continuity equation, motion equation, law of conservation of energy, and heat transfer theory. The result showed that the high friction and low viscosity of CO_2 limited the increase in the injection rate and ratio. Middleton et al. (2015) theorized and outlined the potential advantages including enhanced fracture propagation, reduction in the flow-blocking mechanisms, and increased desorption of adsorbed methane (Xidong et al. 2019; Zhao et al. 2018a). In brief, using supercritical CO_2 as the fracturing fluid can enhance gas production and minimize environmental concerns, and there are few theoretical analysis and experimental research on AE characteristics and crack morphology features at different elapsed times. Moreover, the drilling depth and sealing lengths are the critical parameters determining the success and improving range of supercritical CO_2 fracturing. Studies on the drilling depth and sealing length also

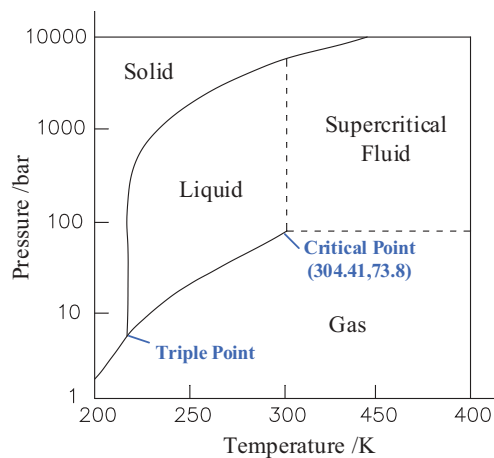


Figure 1. Phase state of carbon dioxide (Zhang et al. 2013).

provide knowledge of small-scale applications or use of supercritical CO₂ in coalmine roadways to displace or recover methane gas or eliminate methane disasters. A reasonable sealing length is required for a successful fracturing, otherwise, it will lead to a waste of time, manpower, and money, or it may endanger the worker safety. Therefore, it is necessary and urgent to improve the theory and technology of supercritical CO₂ fracturing and determine its characteristics at different drilling depths and sealing lengths.

In this study, experimental tests of supercritical CO₂ fracturing at different drilling depths were conducted by a high-precision plunger pump and triaxial loading apparatus with monitoring using an AE instrument. The crack morphology before and after the supercritical CO₂ fracturing was scanned and rebuilt by CT instruments. Damage variables were introduced to analyze the sample damage characteristic. Subsequently, five reasonable stages were proposed based on the damage characteristic, the fracturing fluid pressure curve, and a previous work.

Fracturing experiment

Samples preparation

Shale was the basic material of the supercritical CO₂ fracturing, and the core specimens were taken from similar block shales of the Yibin-Changning district in the south of the Sichuan Basin, as shown in Figure 2. The shale stratum belongs to the Longmaxi formation of the lower Silurian system. The specimens were prepared as cylinders of a size of approximately ϕ 100 mm \times (200 \pm 0.02) mm. The porosity range of the shale sample was from 2.26% to 2.48% with an average of 2.36%, and the uniaxial tensile strength was from 8.8 MPa to 9.5 MPa with an average of 9.17 MPa. The elasticity modulus was



Figure 2. Terrain map of the sampling location.

from 15.08 GPa to 16.48 GPa with an average of 15.97 GPa. The Poisson ratio was from 0.29 to 0.32 with an average of 0.31.

Experimental apparatus

To obtain the pressure and AE of the fracturing process of shale, a high-precision plunger pump of 260D of America TELEDYNE ISCO CO. LTD., PCI-2 AE instrument, triaxial loading system, and constant-temperature control system of an oil bath were used to conduct the laboratory test. This is shown in Figure 2. The volume of the ISCO 260D plunger pump is 266 mL, velocity range is from 0.001 mL/min to 107 mL/min, and pressure range is 10–7500 psi. The maximum axial load stress and confining pressure of the triaxial system are 100 MPa and 15 MPa, respectively, and the maximum displacement of the axial direction and maximum circumference deformation are 60 mm and 10 mm, respectively. The AE device, PCI-2 made by PAC, has the advantages of low noise, multiple channels, low threshold, and good stability, and to achieve high precision, the threshold and collection frequency are set as 40 dB and 150 kHz, respectively.

Experimental scheme

A reasonable drilling depth and sealing length can determine the success of fracturing. To study the effect of the drilling depth and sealing length on supercritical CO₂ fracturing, drilling was conducted with three different sealing lengths for the experimental fracturing. The radius of drilling was 7 mm, radius of the fracturing steel tube was 4 mm, and length of the fracturing chamber was 50 mm. The sealing lengths were 70 mm, 80 mm, and 90 mm, respectively; the interspace between the steel tube and drilling wall was filled with epoxy resin (Figure 3). The stress conditions and injection rates are listed in Table 1.

The experimental procedures can be described as follows:

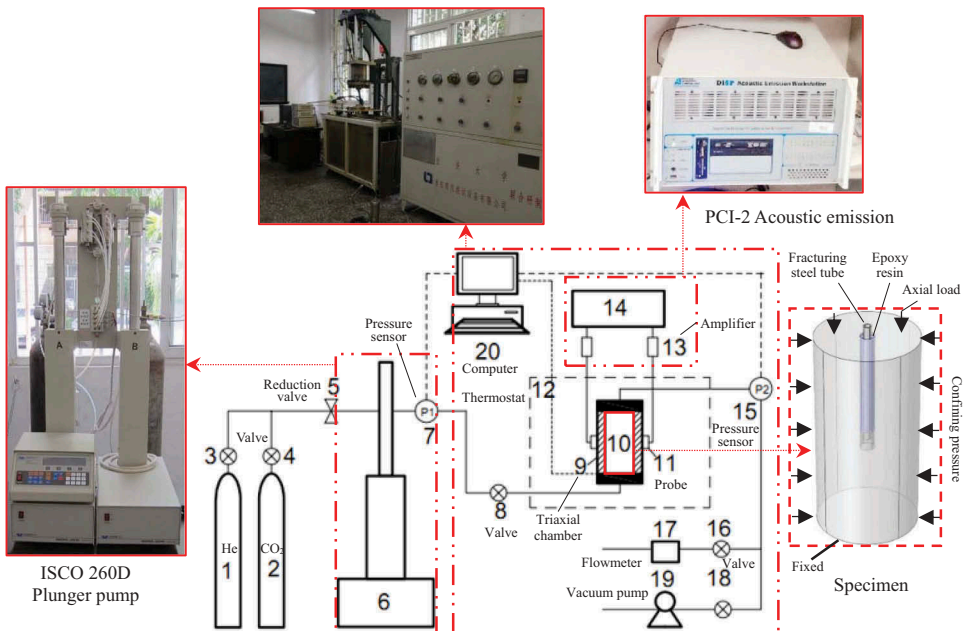


Figure 3. System of supercritical carbon dioxide fracturing.

Table 1. Experimental scheme at different sealing lengths.

Drilling depth	Sealing length	Axial load	Confining pressure	Injection rate
120 mm	70 mm	16 MPa	12 MPa	30 mL/min
130 mm	80 mm	16 MPa	12 MPa	30 mL/min
140 mm	90 mm	16 MPa	12 MPa	30 mL/min

(1) The specimen is prepared as shown in Figure 3 with epoxy resin as the sealing material and a steel tube as the fracturing material. The specimen is painted with silicone rubber to prevent gas leaks.

(2) The specimen is sealed with a heat shrinkable tube, the prepared specimen is installed, and then the test instrument is assembled.

(3) The heat transfer is turned on for the experimental temperature to meet the required condition of supercritical CO₂.

(4) The stress condition is set to reach the experimental scheme.

(5) The specimen is fractured with increasing CO₂ pressure by using pump plungers.

(6) The specimen is scanned after fracturing with CT using a SOMATOM Scope.

Results of supercritical CO₂ fracturing

Fracturing curve

The injected fluid pressure data with the elapsed time were recorded by a pressure transducer, and the representative fracturing curve at each drilling depth was selected, as shown in Figure 4. Three curves show a similar developed rule, but they also exhibit different fluid pressures causing the sample failure. The different states of CO₂ are marked with different colors, and it can be clearly seen that all the failure pressures exceed the supercritical pressure of 7.38 MPa at an appropriate experimental temperature. This shows that the experimental process has reached the required conditions of supercritical CO₂ fracturing. The injected pressure increases until the specimen structural instability and then decreases immediately. The complete

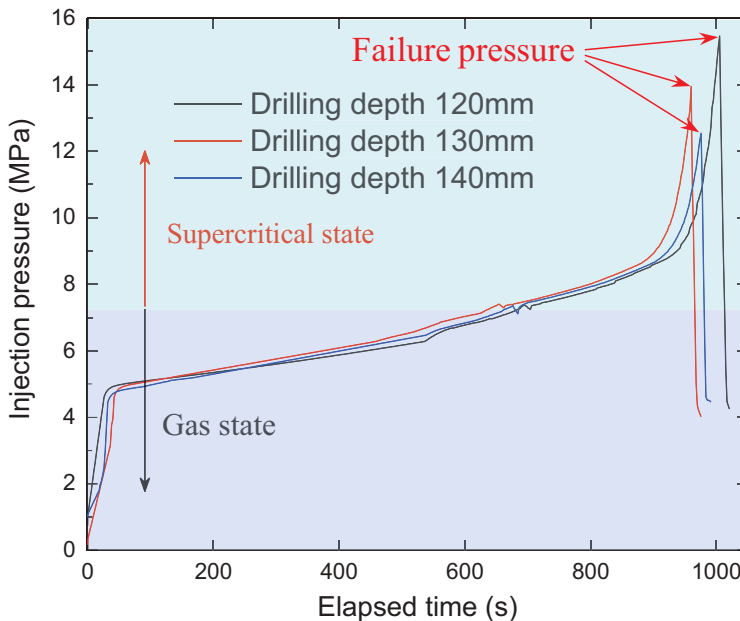


Figure 4. Injection CO₂ pressure vs. the elapsed time.

fracturing process can be described as follows: first the gas pressure mainly dramatically accumulates in the fracturing borehole owing to the gas compressibility. Then, the fluid containing a two-phase stage mainly migrates and accumulates in the shale matrix owing to the fluid increase rate being higher than the fluid migration rate in the shale matrix. Finally, the fluid pressure dramatically increases and then decreases sharply, and a structural failure occurs in the shale matrix because of the sharp change in the fluid pressure. The rapid increase in the pressure is caused by the fluid compressibility reaching its limit in this scenario. However, these pressure curves show some differences, such as in the breakdown pressure, pressure accumulated rate, and time of breakdown point, because of the difference in the experimental conditions.

Relation between drilling depth and failure pressure

An appropriate drilling depth and sealing length are the critical parameters for determining the success and effect of supercritical CO₂ fracturing (Ge et al. 2015). Therefore, the relation between the drilling depth, sealing length, and failure pressure is obtained, as shown in Figure 5. It can be easily found that the failure pressure decreases with the increase in the borehole length and sealing length. This may be attributed to the excavating damage zone of the borehole. To verify the effect of the borehole excavating damage zone on the fracturing failure pressure, numerical experiments of the borehole drilling were conducted by introducing the fast Lagrangian analysis of the continua (FLAC). The numerical model can be simplified as Figure 6. The plastic zone is one of the factors for assessing the failure mode, propagation of the fracturing crack, and effect zone of the pore pressure (Yin 2014). Thus, the Mohr–Coulomb (M–C) failure criterion was used to estimate and obtain the development of the plastic zone (Labuz and Zang 2012). All the numerical stress conditions were similar to the experimental test conditions. The parameter in the numerical model was obtained from the basic mechanical properties test, as given in Table 2. The plastic zone can be used for representing the excavating damage zone in the numerical model based on the M–C criterion. Therefore, in the numerical model, the excavating damage zone can be calculated as shown in Figure 7. It can be found that the damage zone is larger at a deeper drilling depth, and the damage zone around the fracturing chamber at a deeper drilling depth is larger than at other

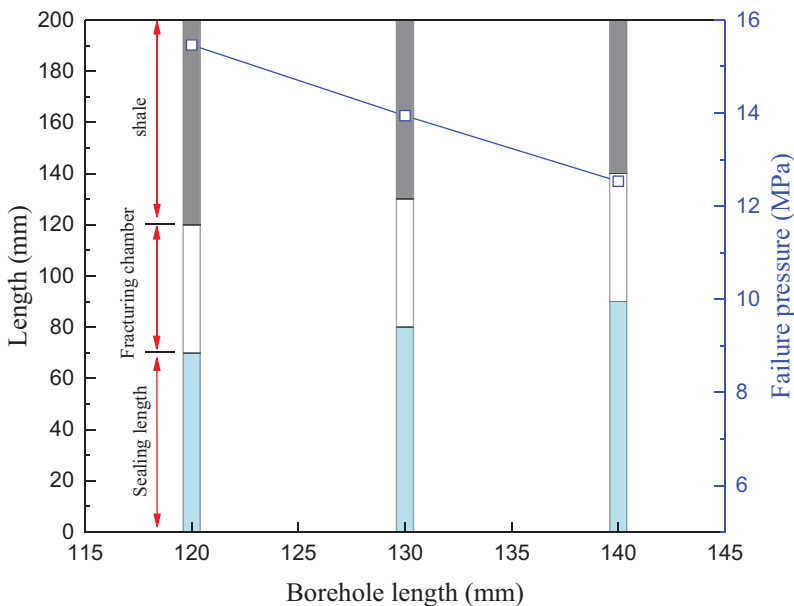


Figure 5. Relation between the failure pressure and borehole length.

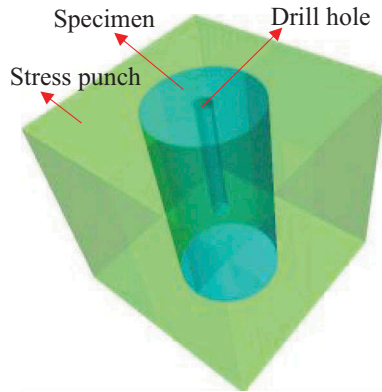


Figure 6. Schematic of the drill hole.

Table 2. Parameters in the numerical model.

Parameter	Value
Elasticity modulus	15.97 (GPa)
Poisson ratio	0.31
Internal friction angle	26.28 (°)
Cohesion	1.74 (MPa)
Tensile strength	9.17 (MPa)

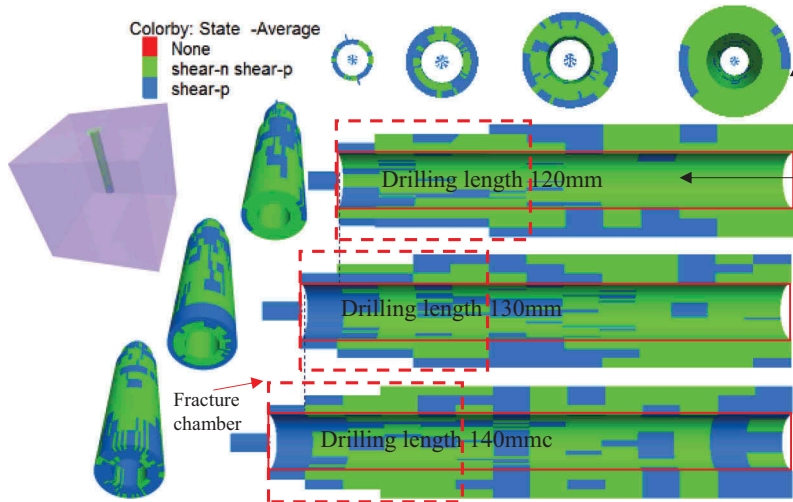


Figure 7. Distribution of the excavating damage zone at different drilling depths.

locations. These are the main reasons for the decrease in the failure pressure with increasing borehole length. Based on the stress contour, plastic zone distribution, and elastic strain softening model (Li et al. 2015a), the zone characteristic around the borehole can be obtained, as exhibited in Figure 8. The initial stress balance status is broken due to the borehole drilling, the stress redistributes, and the limit stress balance point shifts away from the borehole. The new limit stress balance point divides the zone around the borehole into two main parts: damage zone and elastic zone. The damage zone can be divided into partial damage and micro-damage parts based on the plastic zone obtained by the numerical computation. In comparison, the elastic zone can be divided

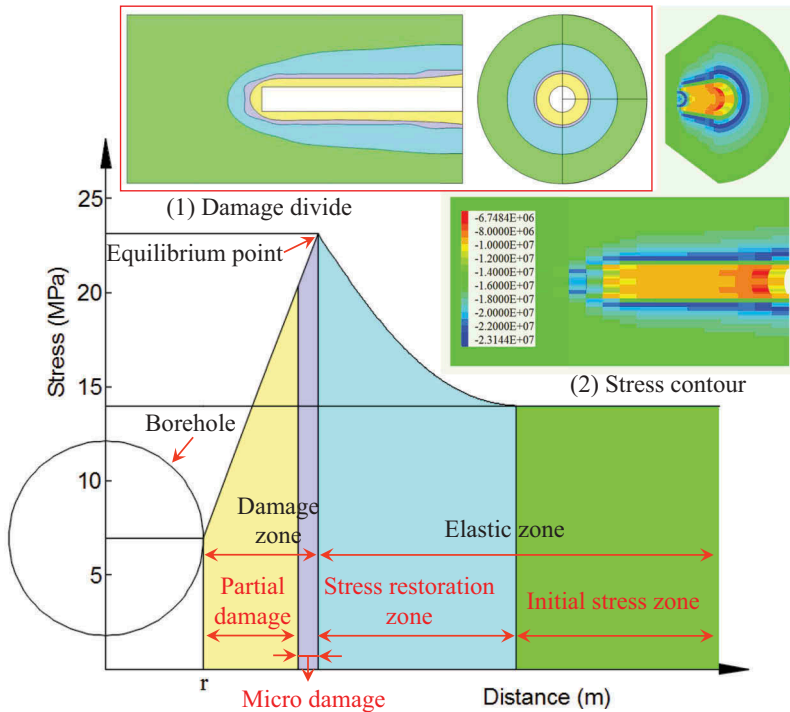


Figure 8. Zone characteristic around the borehole.

into the stress restoration zone and initial stress zone. It is not difficult to note that a damage zone with a “U” shape is formed around the borehole, as depicted in Figure 8 (1). The damage zone is one of the main reasons for the structural failure in the fracturing experiment, whereas the partial damage zone of the damage zone is majorly responsible for the shale structure failure. Therefore, an appropriate control of the damage zone can affect the fracturing result and effect.

Phase change

The sample held in the chamber is kept in a high-temperature oil bath system with the temperature set as 39 °C. With increase in the fluid pressure caused by the plunger pump, the fluid state of CO₂ is changed to a supercritical state from a gas state. It can be clearly found that the fluid pressure shows saltation in the fluid phase change process based on the experimental data, as shown in Figure 9. To determine the reason for the pressure saltation, the basic properties of the density, viscosity, isotherm compression, isothermal expansion, and Adi. bulk modulus can be calculated and obtained with the constant critical temperature based on the equation of state, as shown in Figure 10 (Span and Wagner 1996). It can be found that the density, viscosity, and bulk modulus of CO₂ increase with the pressure increase and dramatic growth of the density, viscosity, and bulk modulus occurring around the supercritical fluid pressure. Obviously, the phase change of CO₂ should be responsible for the dramatic increases in the density, viscosity, and bulk modulus. However, the pressure saltation in the experimental test cannot be directly explained by these dramatic increases in the three parameters. In comparison, the isotherm compression and isothermal expansion show different development tendencies compared to those of the other three mentioned above. The isothermal expansion curve shows a ‘V’ shape, and its value reaches the minimum of 0.04038 when the fluid pressure is at the supercritical point. This illustrates that the CO₂ fluid expands poorly or even

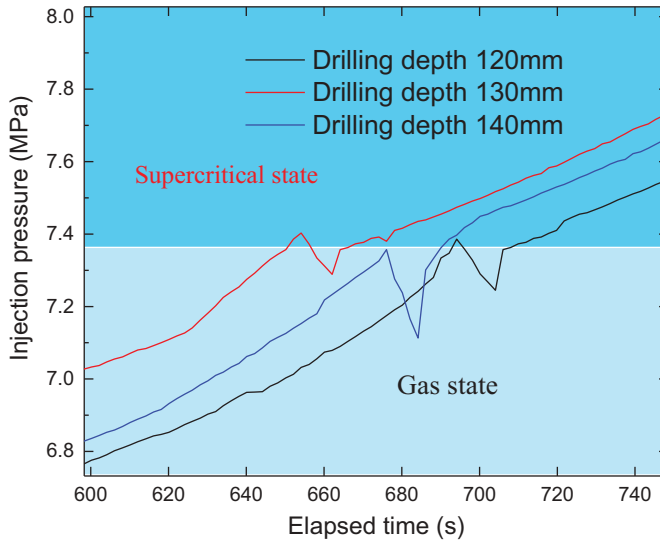


Figure 9. Pressure saltation in the fluid phase change.

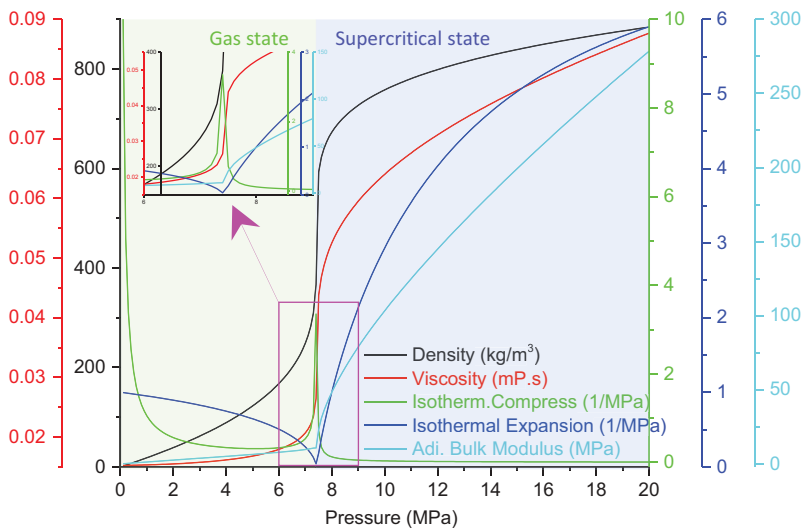


Figure 10. change of CO_2 basic property with gas pressure increasing.

barely expands around the supercritical point of the fluid pressure. In addition, the compression isotherm shows a ‘ \wedge ’ shape, and its value leads to a second peak around the supercritical point, which illustrates that the CO_2 fluid can be compressed early at this point. Overall, the CO_2 fluid possesses a poor isothermal expansion property and good property of isotherm compression around the phase change point. Therefore, the fluid pressure saltation of the test data around the supercritical point can be attributed to the change in the isotherm compression and isothermal expansion.

AE characteristics

Transient elastic waves are generated by the rapidly releasing energy of a local rock failure, and this signal can be detected by an AE instrument (Chen et al. 2015). The AE characteristics were

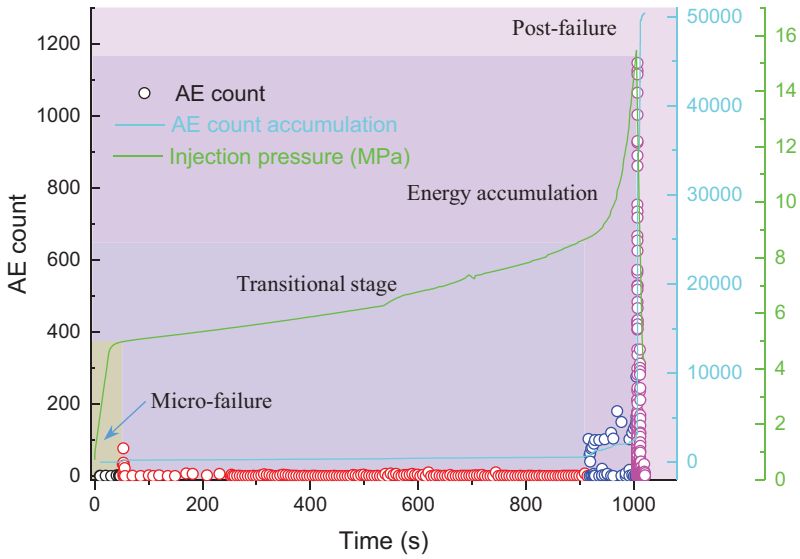


Figure 11. AE characteristics at a drilling depth of 120 mm.

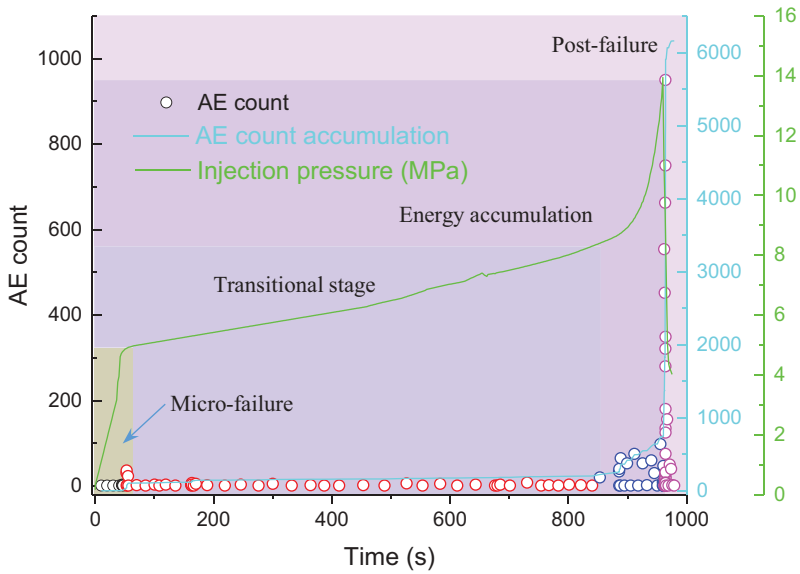


Figure 12. AE characteristics at a drilling depth of 130 mm.

obtained by the instrument, PCI-2 acoustic emission, for the supercritical CO₂ fracturing process, as shown in Figures 11–13. The AE characteristic of the three types of fracturing curves show a similar development tendency, but differences can be found in certain details. Based on the four colors of the AE count and AE count accumulation, the entire fracturing process can be divided into four stages as follows. The first stage of fracturing, defined as micro-failure, shows a micro failure of the plastic damage zone generated by the borehole excavation with a small AE count signal and the gas pressure mainly accumulating in the fracturing chamber, an initial

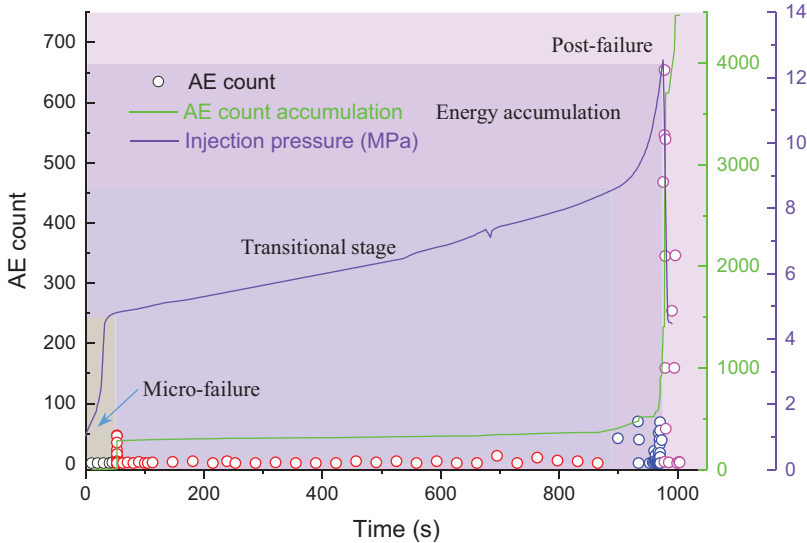


Figure 13. AE characteristics at a drilling depth of 140 mm.

fissure, and a micro-crack induced by the excavation. The second stage, the transitional stage, shows an inconspicuous AE signal without obvious structure failure and yielding. The third stage, energy accumulation, shows a sharp accumulation of the fluid pressure, obvious AE counts, and an increase in the AE count accumulation with the stage. This AE signal can be explained by the yielding of the part shale due to the rock anisotropy. The fourth stage, the so-called post-failure, shows the strongest AE signal in the entire process caused by the shale structure failure. It also exhibits a dramatic increase in the AE count accumulation. In addition, it can be found that the fracturing process at a smaller drilling depth releases a larger AE count and AE count accumulation, which also illustrates the effect of the drilling depth on the failure pressure. Thus, a shorter drilling depth with less damage needs a larger fluid pressure to force the shale break down, releasing numerous AE signal.

Fracturing crack morphology

The fracturing crack morphology is critical information for the assessment of fracturing effects and crack propagation. To analyze the crack morphology induced by supercritical CO₂ fracturing, the CT instruments of SOMATOM Scope were introduced in the experimental test, as shown in Figure 14. The CT scanning planes were set as the vertical plane and horizontal plane crossing the sample center to compare the change before and after supercritical CO₂ fracturing, as presented in Figure 15. The samples without CO₂ fracturing did not have a discernible natural crack, as shown in Figure 15, whereas some obvious cracks induced by the CO₂ fracturing can be found with a simple crack morphology. These results illustrate that effective crack networks can be generated by supercritical CO₂ fracturing. The three-dimensional crack morphology can be reconstructed based on CT scanning images, as shown in Figure 16. The fissure planes at the three drilling depths were highlighted by transparentizing the shale matrix. It can be found that a sample at a drilling depth of 120 mm forms a smooth fissure plane, whereas some more complex fissure planes can be generated in samples at a drilling depth of 130 mm and 140 mm. This illustrates that a deeper drilling depth can promote crack propagation with a larger damage area induced by the drilling. In general, the crack morphology generated by supercritical CO₂ fracturing is relatively simple.

To quantitatively analyze the crack morphology differences in a sample as well as the differences between samples, ten cutting planes of each sample were extracted from the three-dimensional CT

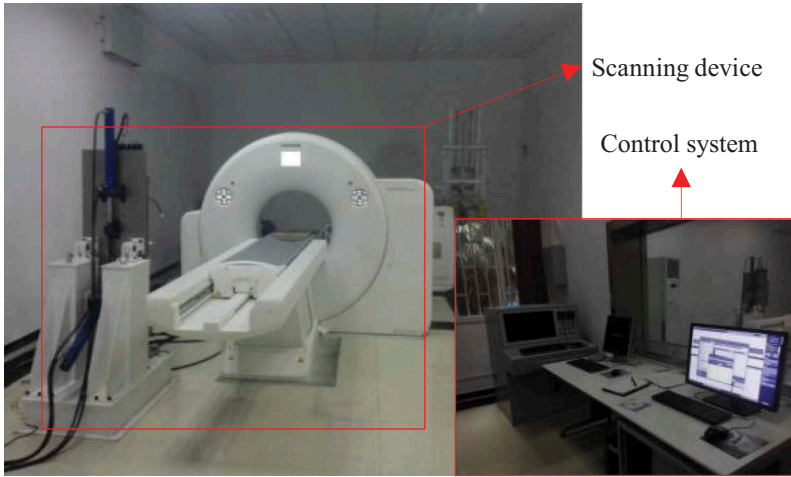


Figure 14. Computed tomography instrument.

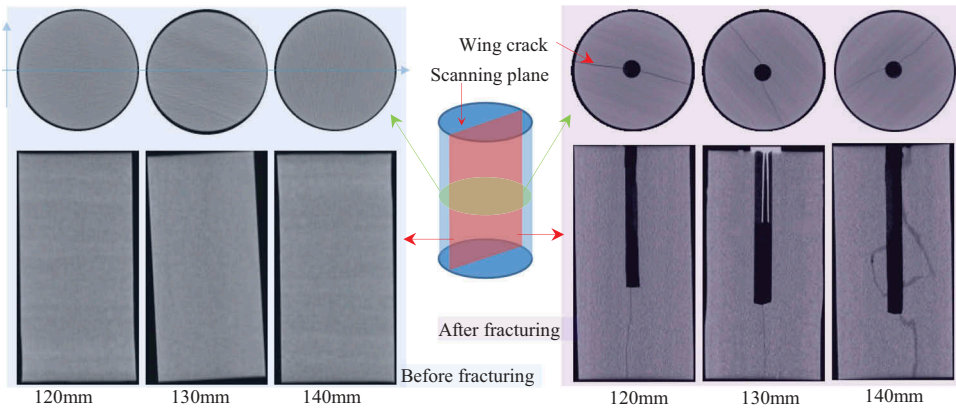


Figure 15. CT comparison before and after CO₂ fracturing.

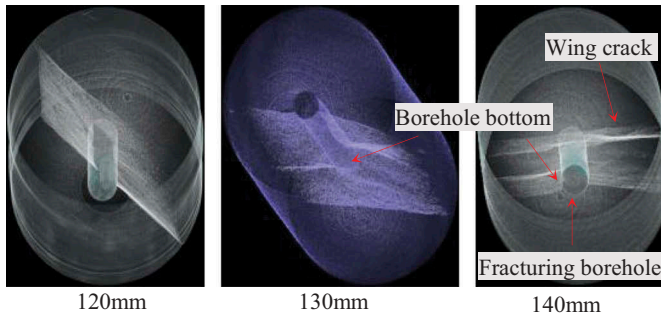


Figure 16. Crack morphology of the three-dimensional reconstruction.

reconstruction model by the AVIZO software. These CT images of the cutting planes were processed by MATLAB with the processing technology of edge detection, image dilation, image filling, and border division. Moreover, the crack quantification characteristics of box-dimension, crack length, and crack area were computed by a self-developed code, as shown in Figure 17. It can be found that the box-

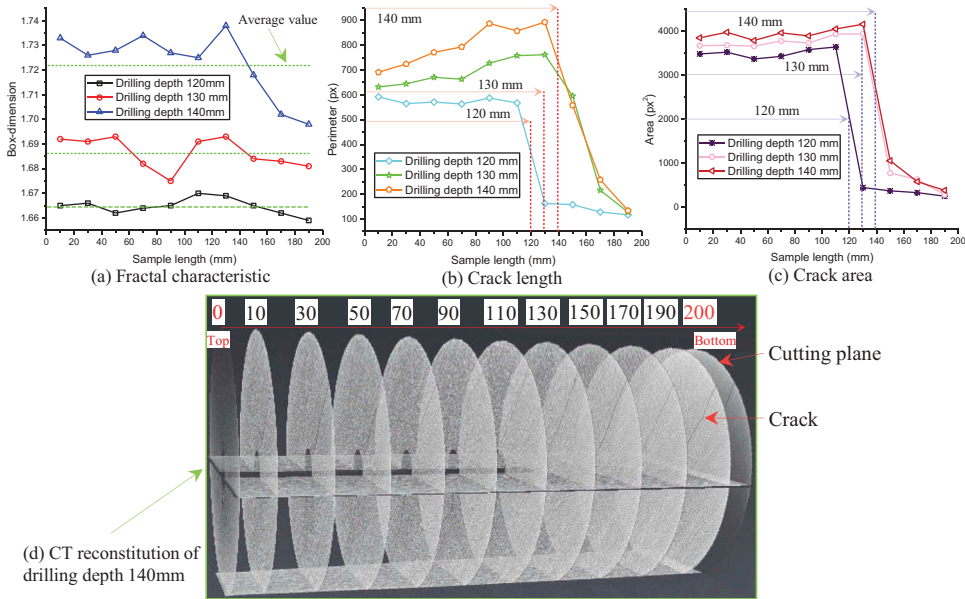


Figure 17. Crack characteristic of the CT scanning plane.

dimension of the three samples exhibits a fluctuation development tendency. The box-dimension average value of the three samples is 1.6647, 1.6865, and 1.7229, respectively, explaining that the crack morphology is more complex at a deep drilling depth. It can also be found that the crack length and area show a sharp drop at the bottom of the fracturing borehole. The main reason is that the area and perimeter of the cutting plane of the borehole are inevitably calculated. The box-dimension, crack length, and crack area of the sample at a drilling depth of 120 mm change slightly despite ignoring the effect of the borehole, illustrating that the crack morphology of each cutting plane is similar, i.e., the fissure plane is relatively flat. This result is in accord with the result shown in Figure 16. Moreover, the crack length and crack area at the sample drilling depth of 130 mm 140 mm increase with the sample length increase at the drilling section, reach maximum at the bottom of the borehole, and then decrease dramatically at the ending of the drilling borehole. These results exhibit that the crack morphology of the sample at a drilling depth of 130 mm 140 mm is more complex at the bottom of the borehole, which matches the exhibition shown in Figure 16. Therefore, it can be assumed that the fracturing crack initial failure occurs at the borehole bottom under these two conditions. Overall, the crack area and crack length of the sample at a drilling depth of 140 mm are larger than those of another sample, illustrating that the crack morphology of a sample at a drilling depth of 140 mm is more complex. In general, the crack morphology is relatively simple, which is slightly different with other research (Zhang et al. 2016).

Discussion

Damage model based on AE characteristic

The AE count can be a good parameter to reflect the change in the mechanical properties due to the release of the strain energy of the material failure and crack propagation based on previous studies (Jiang et al. 2013; Uetsuji and Zako 1998; Yang, Wang, and Qin 2000). Kachanov (1958) proposed a damage variable to assess the damage degree of a material (Kachanov 1999). Thus, a damage variable was introduced to describe the failure of the fracturing process and can be defined as

$$D = \frac{A_d}{A} \tag{1}$$

where A_d is the micro defected area of the bearing surface and A is the bearing area without damage.

If the accumulated AE count of the bearing area, A , with structure failure (complete failure) is C_t , then the AE count of the unit area failure can be obtained as

$$C_u = \frac{C_t}{A} \tag{2}$$

When the damaged area reaches A_d , the accumulated AE count can be obtained as

$$C_d = C_u A_d = \frac{C_t}{A} A_d \tag{3}$$

Therefore, the damage variable based on the AE characteristic can be defined as

$$D = \frac{C_d}{C_t} \tag{4}$$

Owing to the testing machine lacking stiffness and test samples lacking complete failure, the damage variable can be revised as

$$D = D_r \frac{C_d}{C_t} \tag{5}$$

where D_r is the correction coefficient based on the test condition and damage degree of the test sample, and its value ranges from 0 to 1.

Figure 18(a) shows that the AE count accumulation at the three drilling depths shows a similar development tendency; however, some large differences between the extreme values can also be found. Based on the AE count accumulation and theoretical analysis mentioned above, the damage variable at the different drilling depths is obtained as shown in Figure 18(b). It is not difficult to find that a longer drilling depth exhibits a larger initial damage. The main reason for this can be considered that the micro defects induced by the drilling generate a secondary failure caused by the CO₂ fluid pressure in the initial stage. Moreover, a larger damage variable is associated with the micro defects at a longer drilling depth, which is in accordance with the damage zone distribution in the numerical simulation. Based on the analysis of the three damage variable curves, the evolution of the damage variable can be idealized as shown in Figure 18(c). The evolution process of the damage variable can be divided into four parts based on its increase rate. The initial stage with a secondary damage in the micro defects shows a low increase rate of the damage variable. The second stage, the stabilization stage, shows the lowest increase rate of the damage variable. The third stage, progressive failure stage, shows a gradual increase in the increase rate of the damage variable. The fourth stage, structural failure stage, shows the maximal increase rate of the

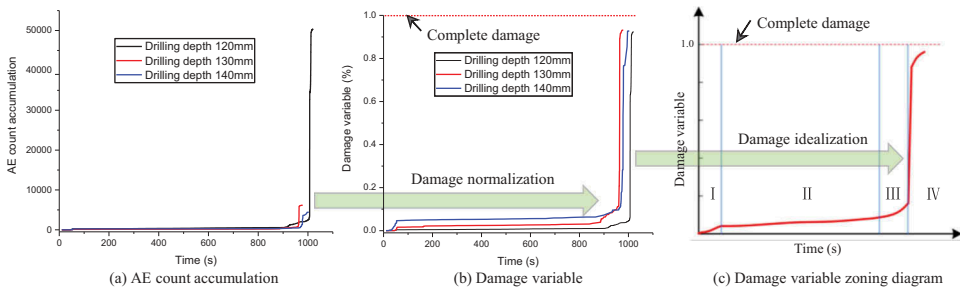


Figure 18. Relationship between the damage variable and elapsed time.

damage variable. This evolution of the damage variable can better illustrate the progressive failure process of supercritical CO₂ fracturing and quantitatively analyze shale damage.

Typical fracturing curve of supercritical carbon dioxide

Supercritical CO₂ fracturing has been introduced as the main non-aqueous fracturing technology to replace hydraulic fracture for better environmental protection and energy saving (Liu et al. 2014). There exists some valuable research work on supercritical CO₂ fracturing, which exhibit a slightly similar development trend as shown in Figure 19 (Inui et al. 2014; Zhang et al. 2016). All the pressure curves are expected to change the development direction, and the pressure increase rate increases sharply at the phase state supercritical point owing to the saltation change of the density and viscosity. Therefore, the supercritical CO₂ fracturing process can be summarized as Figure 20 based on the zoning characteristics and damage features.

Moreover, the entire process of supercritical CO₂ fracturing can be divided into five main stages: gas pressure buildup in the crack and fracture chamber, gas increase and penetration in the skeleton, supercritical CO₂ pressure slow accumulation in the shale matrix, supercritical CO₂ pressure sharp accumulation in the shale matrix, and shale structure failure. Stage I mainly shows that the CO₂ gas pressure primarily accumulates in fracture chamber, joints, and crack induced by the drilling process, and some secondary damage can be found based on the initial damage generated by the drilling process. Stage II shows the characteristic of gas pressure accumulation in the shale matrix with little matrix damage. Stage III mainly illustrates that the supercritical CO₂ pressure accumulates in the shale matrix with little matrix damage. Stage IV shows that the supercritical CO₂ pressure

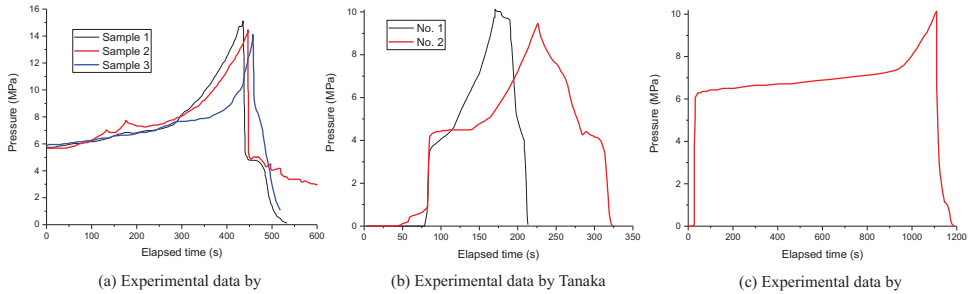


Figure 19. Previous works on fracturing curves (Inui et al. 2014; Zhang et al. 2016).

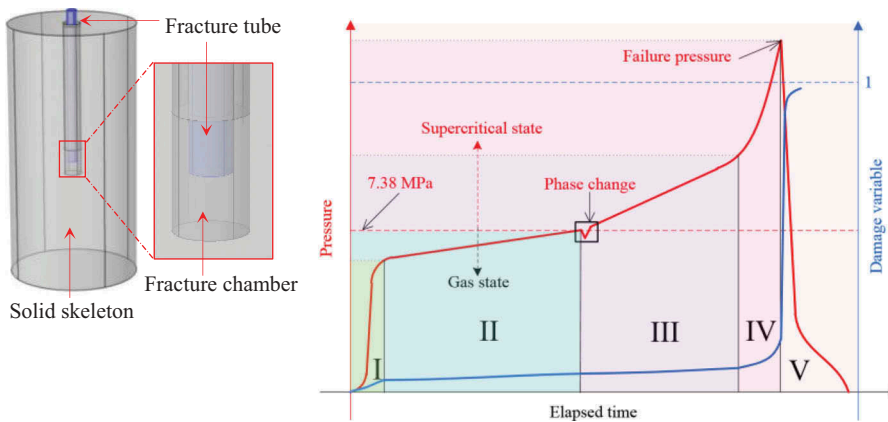


Figure 20. Zoning sketch map of supercritical CO₂ fracturing.

accelerates its accumulation in the shale matrix with an accelerated damage rate, which suggests that the shale matrix may be subject to structure failure. Stage V is the stage of structural failure and post-failure, which shows a dramatical drop in the CO₂ fluid pressure and a sharp damage. It also can be found that the damage variable increases dramatically, and its value is close to 1, but not 1, which is mainly owing to the effect of the shale residual strength without complete damage. The entire process can be divided clearly with definite division points, and the division is also based on previous works. Therefore, the division of the fracturing process is scientific and significant.

Chemical reaction between the shale matrix and supercritical CO₂

It is well known that the pore structure, gas storage capability, and mechanical property of shale can be influenced by the mineral composition (Li et al. 2015b). Nevertheless, the mineral composition can also affect the using and implementing of a reservoir simulation technology owing to the chemical reaction between the reservoir matrix and fracturing fluid. Therefore, the mineral composition is an essential parameter to research and develop a reservoir simulation technology for supercritical CO₂ fracturing. By X-ray diffraction (XRD) and using an adiabatic method, the mineral composition can be obtained as shown in Figure 21 and listed in Table 3. It is not difficult to find that quartz, illite, and dolomite exhibit an obvious intensity in the XRD patterns, which indicates that these three types of minerals occupy a major percentage. In addition, from the mineral composition in Table 3, the content percentage of quartz, calcite, illite, dolomite, and chlorite is 65.4%, 6.25%, 9.8%, 6.87%, and 6.59%, respectively. The remaining mineral composition is 5.09%. The mineralogical constituents are quite similar. Overall, the analyzed specimen is characterized by relatively high brittle mineral contents, which is in accordance with previous research (Tan et al. 2014). The main chemical constituent of quartz is SiO₂, which is relatively chemically stable, indicating that silica does not react with water and a typical acid. Moreover, the main constituent of calcite, dolomite, illite, and chlorite is CaCO₃, CaMg(CO₃)₂, K_{0.6}Mg_{0.25}Al_{1.8}(Al_{0.5}Si_{3.5}O₁₀)(OH)₂, and Mg_{2.5}Fe_{2.5}Al₂Si₃O₁₀(OH)₈, respectively. These those constituents are not stable, indicating that they may react to some degree with the weak acid formed by the injected CO₂ (Yang et al. 2014).

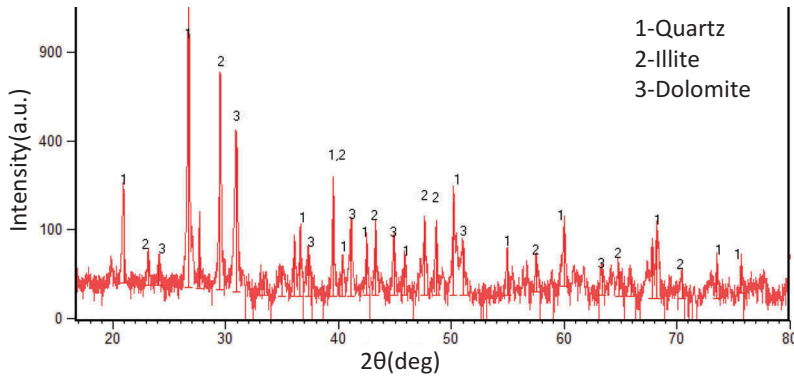


Figure 21. XRD patterns of the shale specimen.

Table 3. Mineral composition.

Component	Content (%)
Quartz	65.4
Calcite	6.25
Illite	9.8
Dolomite	6.87
Chlorite	6.59
Others	5.09

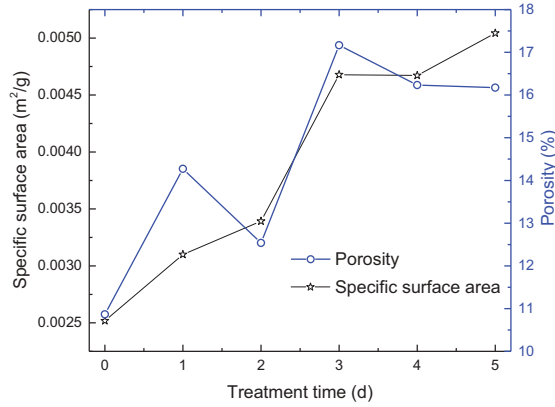
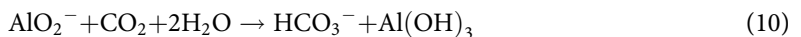
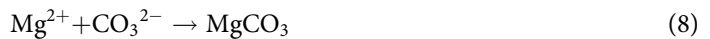


Figure 22. Time effect on the shale specific surface and porosity (Jiang et al. 2016).

Supercritical CO₂ fracturing is a complex process to improve shale reservoir permeability, which competes with the complex fluid–mechanical coupling process and fluid–matrix chemical reaction process. If the time effect is considered in the fracturing process, the chemical reaction between the fracturing fluid and shale becomes more complex. By processing and analyzing previous studies (Jiang et al. 2016), the effect of the treatment time of the shale immersion in supercritical CO₂ on the specific surface area and porosity can be obtained as shown in Figure 22. It is obvious that the specific surface area and porosity increase on adding treatment time to the mass, whereas the porosity shows some fluctuation. The reason for the increased specific surface area and porosity is the sufficient dissolving capability of supercritical CO₂. In comparison, the dissolving capability is owing to the reaction between the shale matrix and supercritical CO₂. When CO₂ is injected into a shale reservoir, the coexisting CO₂ (gas) and CO₂ (liquid) encounter the moisture in the matrix and formation, and H⁺, HCO₃⁻, and CO₃²⁻ are provided by this ‘meeting’ reaction, as shown in equations (6–7).



In addition, Mg²⁺, Fe²⁺, Al³⁺, Fe³⁺, and AlO₂⁻ ions can be obtained from the solution of calcite, illite, dolomite, and chlorite. These types of ions are the key minerals of the reaction between the CO₂–H₂O–matrix for providing the raw material for the precipitation of carbonate minerals.



The oxides, MgO, K₂O, Na₂O, and CaO, can also react with CO₂ and H₂O, producing the precipitates of Mg₂(OH)₂CO₃, Ca(HCO₃)₂, KHCO₃, NaHCO₃, and CaCO₃. These reactions between the shale matrix and supercritical CO₂ can dissolve and remove substances that hinder shale pores, such as clay and carbonates, improving the shale porosity and connectivity. A complete contact between the supercritical fluid and matrix can increase the displacement gas in the shale pore and gas desorption from the shale pore surface. Supercritical CO₂ not only influences the shale micro-structure in terms of the porosity and specific surface area but also the shale surface chemical

properties of water wettability and surface tension (Qin et al. 2017). With a longer treatment time of supercritical CO₂ fracturing, the chemical reaction between CO₂ and the shale solid skeleton will be more sufficient. The reaction contact between a supercritical fluid and shale is more sufficient compared to that with other improving fluids, which makes it easier to expel the clogging impurities from the pores, thereby improving the porosity and pore connectivity and increasing the drainage of shale gas and gas desorption (Lu et al. 2015). Therefore, for better reservoir simulation, the time effect should be considered when supercritical CO₂ fracturing is implemented for shale gas extraction.

Conclusions

Supercritical carbon dioxide experiments were conducted to determine the influence of drilling depths, and acoustic emission signals were also recorded. In addition, the crack morphologies were scanned by CT before and after the fracturing experiment. Moreover, the damage model, fracturing curve, and chemical reaction were analyzed and discussed. Based on the above work, the following conclusions were drawn:

(1) The structure failure pressure decreased with the increase in the borehole length and sealing length, which was due to the larger excavation damage zone at deeper drilling depths. Moreover, the region around the borehole could be divided into four parts: partial damage zone, micro-damage zone, stress restoration zone, and initial stress zone, based on the damage and stress conditions.

(2) The saltation of the fracturing curves was due to the phase change of carbon dioxide, which was critically led by the change in the isotherm compression and isothermal expansion. The acoustic emission characteristics of the fracturing experiments showed a similar development trend, which could be divided into four stages of micro-failure, transactional stage, energy accumulation, and post-failure.

(3) Comparison of the crack morphology before and after the fracturing experiments showed that supercritical carbon dioxide could generate an obvious 'wing' crack. A complex crack could be formed at a deeper drilling depth, as revealed by the comparisons of the box dimension, crack perimeter, and crack area at different drilling depths.

(4) Based on previous works and the damage characteristic and fluid pressure features, the entire process of supercritical carbon dioxide fracturing could be divided into five main stages: gas pressure buildup in the crack and fracture chamber, gas pressure accumulation in the shale matrix, supercritical phase pressure accumulation in the shale matrix, supercritical carbon dioxide pressure accelerated accumulation in the shale matrix, structural failure, and post-failure. Supercritical CO₂ could dissolve and remove substances, improving the shale porosity and connectivity.

Conflict of Interest

The authors declare no competing financial interest.

Funding

This work was supported by the National Natural Science Foundation of China [51474039, 51404046, 51904043 and U1361205]; Natural Science Foundation of Hunan Province (2019JJ50150), China Postdoctoral Science Foundation (2018M641366) and Scientific Research Foundation of State Key Laboratory of Coal Mine Disaster Dynamics and Control (2011DA105287-ZD201302 and 2011DA105287-MS201403); China Postdoctoral Science Foundation [2018M641366]; National Natural Science Foundation of China [51474039, 51404046 and U1361205]; Natural Science Foundation of Hunan Province [2019JJ50150]; and Scientific Research Foundation of State Key Laboratory of Coal Mine Disaster Dynamics and Control [2011DA105287-ZD201302 and 2011DA105287-MS201403].

ORCID

Yuan Zhao  <http://orcid.org/0000-0001-7990-5141>

References

- Cao, P., J. S. Liu, and Y. K. Leong. 2016. A fully coupled multiscale shale deformation-gas transport model for the evaluation of shale gas extraction. *Fuel* 178:103–17. doi:10.1016/j.fuel.2016.03.055.
- Chen, G. Q., Y. Zhang, R. Q. Huang, et al. 2015. Failure mechanism of rock bridge based on acoustic emission technique. *Journal of Sensors*
- Cheng, Y., G. Li, H. Wang, et al. 2013. Pressure boost mechanism within cavity of the supercritical CO₂ jet fracturing. *Acta Petrolei Sinica* 34 (3):550–55.
- Cheng, Y., G. Li, H. Wang, et al. 2014. Phase control of wellbore fluid during supercritical CO₂ jet fracturing. *Acta Petrolei Sinica* 35 (6):1182–87.
- Du, Y., R. Wang, H. Ni, et al. 2011. The research and development of supercritical carbon dioxide wellbore flow characteristics analysis system. *Electronic Journal of Geotechnical Engineering* 16:1581–92.
- Fang, C., W. Chen, and M. Amro. 2014. *Simulation study of hydraulic fracturing using super critical CO₂ in Shale*. Abu Dhabi International Petroleum Exhibition and Conference, Abu Dhabi, UAE.
- Ge, Z. L., X. D. Mei, Y. Y. Lu, J. Tang, and B. Xia. 2015. Optimization and application of sealing material and sealing length for hydraulic fracturing borehole in underground coal mines. *Arabian Journal of Geosciences* 8 (6):3477–90. doi:10.1007/s12517-014-1488-6.
- Guo, J., and J. Zeng. 2015. A coupling model for wellbore transient temperature and pressure of fracturing with supercritical carbon dioxide. *Acta Petrolei Sinica* 36 (2):203–09.
- Inui, S., T. Ishida, Y. Nagaya, Y. Nara, Y. Chen, Q. Chen. 2014. *AE monitoring of hydraulic fracturing experiments in granite blocks using supercritical CO₂, water and viscous oil*. 48th U.S. Rock Mechanics/Geomechanics Symposium, Minneapolis, Minnesota.
- Ishida, T., K. Aoyagi, T. Niwa, Y. Chen, S. Murata, Q. Chen, and Y. Nakayama. 2012. Acoustic emission monitoring of hydraulic fracturing laboratory experiment with supercritical and liquid CO₂. *Geophysical Research Letters* 39:n/a-n/a. doi:10.1029/2012GL052788.
- Jiang, D., J. Chen, S. Ren, X. Yuan, C. Yang. 2013. *A damage constitutive model of rock salt based on acoustic emission characteristics*. Clean Energy Systems in the Subsurface: Production, Storage and Conversion, Springer Berlin Heidelberg. Goslar, Germany. 363–77.
- Jiang, Y. D., Y. H. Luo, Y. Y. Lu, C. Qin, and H. Liu. 2016. Effects of supercritical CO₂ treatment time, pressure, and temperature on microstructure of shale. *Energy* 97:173–81. doi:10.1016/j.energy.2015.12.124.
- Kachanov, L. M. 1958. Time of the rupture process under creep conditions. *Izv Akad Nauk S S R Otd Tech Nauk* 8:26–31.
- Kachanov, L. M. 1999. Rupture time under creep conditions. *International Journal of Fracture* 97 (1):11–18. doi:10.1023/A:1018671022008.
- Kubala, G., and B. A. Mackay. 2010. *Use of carbon-dioxide-based fracturing fluids*. US Patent.
- Labuz, J. F., and A. Zang. 2012. Mohr–Coulomb failure criterion. *Rock Mechanics & Rock Engineering* 45 (6):975–79. doi:10.1007/s00603-012-0281-7.
- Li, Y., S. G. Cao, N. Fantuzzi, and Y. Liu. 2015a. Elasto-plastic analysis of a circular borehole in elastic-strain softening coal seams. *International Journal of Rock Mechanics and Mining Sciences* 80:316–24. doi:10.1016/j.ijrmms.2015.10.002.
- Li, Y., Y. Li, B. Wang, Z. Chen, and D. Nie. 2016. The status quo review and suggested policies for shale gas development in China. *Renewable & Sustainable Energy Reviews* 59:420–28. doi:10.1016/j.rser.2015.12.351.
- Li, Y. J., X. Y. Li, Y. L. Wang, and Y. Qingchun. 2015b. Effects of composition and pore structure on the reservoir gas capacity of carboniferous shale from Qaidam Basin, China. *Marine and Petroleum Geology* 62:44–57. doi:10.1016/j.marpetgeo.2015.01.011.
- Liteanu, E., and C. J. Spiers. 2011. Fracture healing and transport properties of wellbore cement in the presence of supercritical CO₂. *Chemical Geology*, 281 (3–4):195–210.
- Liu, H., F. Wang, J. Zhang, S. MENG, and Y. DUAN. 2014. Fracturing with carbon dioxide: Application status and development trend. *Petroleum Exploration and Development* 41 (4):513–19. doi:10.1016/S1876-3804(14)60060-4.
- Lu, Y. Y., F. Yang, Z. L. Ge, S. Wang, and Q. Wang. 2015. The influence of viscoelastic surfactant fracturing fluids on gas desorption in soft seams. *Journal of Natural Gas Science and Engineering* 27:1649–56. doi:10.1016/j.jngse.2015.10.031.
- Middleton, R., H. Viswanathan, R. Currier, and R. Gupta. 2014. CO₂ as a fracturing fluid: Potential for commercial-scale shale gas production and CO₂ sequestration. *Energy Procedia* 63:7780–84. doi:10.1016/j.egypro.2014.11.812.
- Middleton, R. S., J. W. Carey, R. P. Currier, J. D. Hyman, Q. Kang, S. Karra, J. Jiménez-Martínez, M. L. Porter, and H. S. Viswanathan. 2015. Shale gas and non-aqueous fracturing fluids: Opportunities and challenges for supercritical CO₂. *Applied Energy* 147:500–09. doi:10.1016/j.apenergy.2015.03.023.
- Qin, C., Y. Jiang, Y. Luo, X. Xian, H. Liu, and Y. Li. 2017. Effect of supercritical carbon dioxide treatment time, pressure, and temperature on shale water wettability. *Energy & Fuels* 31 (1):493–503. doi:10.1021/acs.energyfuels.6b03257.

- Span, R., and W. Wagner. 1996. A new equation of state for carbon dioxide covering the fluid region from the triple-point temperature to 1100 K at pressures up to 800 MPa. *Journal of Physical and Chemical Reference Data* 25 (6):1509–96. doi:10.1063/1.555991.
- Stephenson, M. H. 2016. Shale gas in North America and Europe. *Energy Science & Engineering* 4 (1):4–13. doi:10.1002/ese3.96.
- Sun, M., B. Yu, Q. Hu, Y. Zhang, B. Li, R. Yang, Y. B. Melnichenko, and G. Cheng. 2017. Pore characteristics of Longmaxi shale gas reservoir in the Northwest of Guizhou, China: Investigations using small-angle neutron scattering (SANS), helium pycnometry, and gas sorption isotherm. *International Journal of Coal Geology* 171:61–68. doi:10.1016/j.coal.2016.12.004.
- Tan, J., P. Weniger, B. Krooss, A. Merkel, B. Horsfield, J. Zhang, C. J. Boreham, G. V. Graas, and B. A. Tocher. 2014. Shale gas potential of the major marine shale formations in the upper yangtze platform, South China, Part II: Methane sorption capacity. *Fuel* 129 (4):204–18. doi:10.1016/j.fuel.2014.03.064.
- Uetsuji, Y., and M. Zako. 1998. On evaluation procedure to AE test for fiber reinforced composite materials based on damage mechanics. *Transactions of the Japan Society of Mechanical Engineers* 64 (628):2938–44. doi:10.1299/kikaia.64.2938.
- Wang, H., G. Li, and Z. Shen. 2012. A feasibility analysis on shale gas exploitation with supercritical carbon dioxide. *Energy Sources Part A Recovery Utilization & Environmental Effects* 34 (15):1426–35. doi:10.1080/15567036.2010.529570.
- Wang, Q., and R. R. Li. 2016. Natural gas from shale formation: A research profile. *Renewable & Sustainable Energy Reviews* 57:1–6. doi:10.1016/j.rser.2015.12.093.
- Xidong, D., G. Min, L. Zhenjian, Y. Zhao, F. Sun, and T. Wu. 2019. Enhanced shale gas recovery by the injections of CO₂, N₂, and CO₂/N₂ mixture gases. *Energy & Fuels* 33 (6):5091–101. doi:10.1021/acs.energyfuels.9b00822.
- Xu, C. Y., Y. L. Kang, Z. J. You, and M. Chen. 2016. Review on formation damage mechanisms and processes in shale gas reservoir: Known and to be known. *Journal of Natural Gas Science and Engineering* 36 (B):1208–19. doi:10.1016/j.jngse.2016.03.096.
- Yang, G., Y. Li, M. Xin, J. Dong. 2014. Effect of Chlorite on CO₂-water-rock interaction. *Earth Science* 39 (4):462–72.
- Yang, J. H., F. W. Wang, and S. Y. Qin. 2000. Experimental and theoretical study on AE characteristic and damage model of HTPB composite solid propellant. *Journal of Solid Rocket Technology*. 23 (3):37–40.
- Yap, N. T. 2016. Unconventional shale gas development: Challenges for environmental policy and EA practice. *Impact Assessment and Project Appraisal* 34 (2):97–109. doi:10.1080/14615517.2016.1176405.
- Yin, N. 2014. Analysis on surrounding rock mass plastic zone of deep underground chamber based on Hoek-Brown Criterion. *Advanced Materials Research* 838–841:741–46. doi:10.4028/www.scientific.net/AMR.838-841.741.
- Yuan, J. H., D. K. Luo, and L. Y. Feng. 2015. A review of the technical and economic evaluation techniques for shale gas development. *Applied Energy* 148:49–65. doi:10.1016/j.apenergy.2015.03.040.
- Zhang, X., Y. Lu, J. Tang, Z. Zhou, Y. Liao. 2016. Experimental study on fracture initiation and propagation in shale using supercritical carbon dioxide fracturing. *Fuel* 190 (15):370–378.
- Zhang, X. T., X. Jiang, J. Y. Yang, and M. Chen. 2015. A newly developed rate analysis method for a single shale gas well. *Energy Exploration & Exploitation* 33 (3):309–16. doi:10.1260/0144-5987.33.3.309.
- Zhang, Y. X., P. F. Wang, J. Yang, and G. Q. Li. 2013. Study on supercritical carbon dioxide fracturing coalbed gas method. *Advanced Materials Research* 807–809:2529–33. doi:10.4028/www.scientific.net/AMR.807-809.
- Zhao, J. Z., C. Y. Liu, H. Yang, and Y. Li. 2015. Strategic questions about China's shale gas development. *Environmental Earth Sciences* 73 (10):6059–68. doi:10.1007/s12665-015-4092-5.
- Zhao, Y., S. Cao, Y. Li, L. Qin. 2015. The analysis of antireflection range in coal seam hydraulic fracturing. *Journal of Mining and Safety Engineering* 32 (4):644–50.
- Zhao, Y., S. Cao, Y. Li, H. Yang, P. Guo, G. Liu, and R. Pan. 2018a. Experimental and numerical investigation on the effect of moisture on coal permeability. *Natural Hazards* 90 (3):1201–21. doi:10.1007/s11069-017-3095-9.
- Zhao, Y., S. Cao, Y. Li, Z. Zhang, P. Guo, H. Yang, S. Zhang, and R. Pan. 2018b. The occurrence state of moisture in coal and its influence model on pore seepage. *RSC Advances* 8 (10):5420–32. doi:10.1039/C7RA09346B.
- Zhao, Y., S. Cao, D. Shang, H. Yang, Y. Yu, Y. Li, J. Liu, H. Wang, R. Pan, H. Yang, et al. 2019. Crack propagation and crack direction changes during the hydraulic fracturing of coalbed. *Computers and Geotechnics* 111:229–42. doi:10.1016/j.compgeo.2019.03.018.
- Zhou, J. P., G. J. Liu, Y. D. Jiang, X. Xian, Q. Liu, D. Zhang, and J. Tan. 2016. Supercritical carbon dioxide fracturing in shale and the coupled effects on the permeability of fractured shale: An experimental study. *Journal of Natural Gas Science and Engineering* 36:369–77. doi:10.1016/j.jngse.2016.10.005.
- Zhu, L. H., J. H. Yuan, and D. K. Luo. 2016. A new approach to estimating surface facility costs for shale gas development. *Journal of Natural Gas Science and Engineering* 36:202–12. doi:10.1016/j.jngse.2016.10.013.
- Zou, C. N., D. Z. Dong, Y. M. Wang, X. LI, J. HUANG, S. WANG, Q. GUAN, C. ZHANG, H. WANG, H. LIU, et al. 2015. Shale gas in China: Characteristics, challenges and prospects (I). *Petroleum Exploration and Development* 42 (6):753–67. doi:10.1016/S1876-3804(15)30072-0.